The crystal structure of $Cd_2Nb_2O_7$: symmetry mode analysis of the ferroelectric phase

2010 J. Phys.: Condens. Matter 22 205401

(http://iopscience.iop.org/0953-8984/22/20/205401)

J. Phys.: Condens. Matter **22** (2010) 205401 (8pp) doi:10.1088/0953-8984/22/20/205401

The crystal structure of $Cd_2Nb_2O_7$: symmetry mode analysis of the ferroelectric phase

T Malcherek, U Bismayer and C Paulmann

Mineralogie, Department Geowissenschaften, Universität Hamburg, Grindelallee 48, 20146 Hamburg, Germany

E-mail: thomas.malcherek@uni-hamburg.de

Received 25 February 2010
Published 26 April 2010
Online at stacks.iop.org/JPhysCM/22/205401

Abstract

The crystal structure of the ferroelectric $Cd_2Nb_2O_7$ (CNO) has been determined down to $T = 98$ K using synchrotron radiation. Low temperature structure refinement is conducted in space group $Ima2$, starting from the crystal structure previously determined by *ab initio* methods. Symmetry mode analysis indicates that the primary order parameter is of T_{2u} symmetry with the largest displacement amplitude at the Nb(2) position. The associated phase transition temperature is obtained as $T_c = 194$ K by extrapolation. Long exposure x-ray diffraction scans confirm the presence of anisotropic diffuse scattering intensity in layers normal to $\langle 110 \rangle_{cub}$ over the entire temperature range. The diffuse scattering intensity significantly decays below $T = 198$ K. The refined thermal parameters indicate that the disorder responsible for the diffuse scattering is primarily associated with Nb.

(Some figures in this article are in colour only in the electronic version)

1. Introduction

Oxide relaxor ferroelectrics such as $PbMg_{1/3}Nb_{2/3}O_3$ (PMN) are commonly based on compositionally disordered ABO_3 perovskite structures [1]. Relaxor behaviour in ferroelectric (FE) materials is characterized by a broad frequency-dependent peak in the real part of the temperature-dependent dielectric susceptibility. In spite of the absence of chemical mixing, $Cd_2Nb_2O_7$ (CNO), a ferroelectric of the pyrochlore structure type [2, 3] shows those typical properties of relaxor materials over a limited temperature range [4]. This presents an opportunity to study the basic principles of relaxor behaviour without the need to address the structural complexities of solid solutions. However, understanding the complex sequence of phase transitions occurring in CNO is fundamental to the understanding of its unusual dielectric properties.

At temperatures above $T_1 = 205$ K CNO is cubic with space group (SG) symmetry $Fd\bar{3}m$. At and below this temperature a total of four phase transitions (PTs) have been confirmed in the recent literature. The transition at T_1 has been classified as improper ferroelectric [5]. Spontaneous polarization has been reported for all temperatures below T_1 [6], albeit with a very small magnitude for $T_2 < T < T_1$. A domain structure with domain walls parallel to the pseudocubic $\langle 100 \rangle$ directions appears below T_1 [5]. The intermediate phase between T_1 and T_2 has also been classified as an improper ferroelastic by some authors. It might belong to either a tetragonal [7] or an orthorhombic [8] crystal system.

A broad heat capacity anomaly and a frequency-dependent dielectric function [4] have been reported at and below $T_2 \approx 195$ K. Both properties are typical features of relaxor ferroelectrics. An incomplete polar soft mode (SM) that couples to a central mode [8] as well as overdamping of the FE-mode [9] have been suggested to explain the measured dielectric properties within the paraelectric phase. More recently an overdamped SM has been observed in a single domain of the FE-phase using confocal micro-Raman spectroscopy [10]. Taking the overdamping and coupling to the central mode into account this mode softens at T_2.

At $T_3 \approx 85$ K a further structural PT has been found, indicated by anomalies in heat capacity and dielectric constant [3, 4, 11]. Below T_3 monoclinic symmetry has been proposed [7].

The occurrence of a first order PT near $T_4 = 46$ K has been confirmed by heat capacity measurements [4]. The crystal structures of the orthorhombic phase, that is supposed to exist

Table 1. Crystal data and refinement details of CNO.

Temperature (K)	292	220	192	160	120	98
Crystal data						
Chemical formula	$Cd_2Nb_2O_7$					
M_r	522.63					
Crystal system, space group	Cubic, $Fd\bar{3}m$		Orthorhombic, $Ima2$			
a (Å)	10.365(1)	10.360(1)	7.324(1)	7.323(1)	7.322(1)	7.322(1)
b (Å)			10.358(1)	10.358(1)	10.356(1)	10.356(1)
c (Å)			7.324(1)	7.324(1)	7.324(1)	7.323(1)
V (Å ^{3})	1113.5(1)	1111.9(1)	555.6(1)	555.5(1)	555.4(1)	555.3(1)
Z	8		4			
Crystal size (mm)	$0.14 \times 0.12 \times 0.09$					
μ (mm^{-1})	11.3	11.3	11.3	11.3	11.6	11.6
λ (Å)	0.709 74					
Refinement data						
R_{merge}	0.063	0.065	0.044	0.038	0.049	0.046
Cond. for obs. reflections	$I > 3\sigma(I)$					
R_{obs}	0.023	0.022	0.035	0.034	0.038	0.04
Goodness of fit	1.25	1.55	1.1	1.26	1.35	1.46
Number of reflections	393	396	8766	8888	9012	9047
Number of parameters	11		59			
Number of domains	1		11			

between T_2 and T_3 and of the monoclinic phase below T_3, have recently been predicted by *ab initio* methods [12].

While there is a substantial body of literature on phase transitions and dielectric properties of CNO (cf references in [4, 6]), very few results of diffraction experiments on CNO have been published so far. Moreover, most of the existing diffraction data is based on powder methods [7, 13]. As the spontaneous strain associated with the phase transitions in CNO is very small, attempts to determine the symmetries and atomic displacements associated with the various phase transitions using powder diffraction are severely hampered by peak overlap. The authors are aware of only one single crystal diffraction study [14], which was not concerned with the ferroelectric state though. The main purpose of the present study is to provide crystal structure data of the ferroelectric phase for $T > T_3$. In addition we report on the temperature dependence of anisotropic diffuse scattering in CNO that was previously described at ambient temperature [15]. The ambient temperature diffuse scattering has very recently been simulated using *ab initio* molecular dynamics and Monte Carlo methods [16].

2. Experimental details

Crystals of CNO have been grown by the flux method [17]. The obtained transparent aggregate of several mm in diameter has light yellow colour, with small fragments appearing colourless. Phase purity was established by x-ray powder diffraction. Electron microprobe analysis confirmed a Cd/Nb ratio of 0.99 ± 0.01. X-ray diffraction measurements have been conducted at Hasylab beamline F1 (Desy/Hamburg) on a small single crystal fragment. A MarCCD 165 detector with 2048 pixels $\times$ 2048 pixels has been used at a wavelength of 0.709 74 Å (1 Å $=$ 0.1 nm). Diffraction maxima have been measured at temperatures 292, 220, 192, 160, 120 and 98 K, using ϕ-scans at four different goniometer and detector settings for each temperature. Temperature was controlled by an Oxford Cryostream 600 device. Raw image data have been corrected for primary beam decay (program SCLMAR). Intensity integration has been performed using XDS [18] with all internal scaling correction methods disabled. In order to account for absorption effects, an effective crystal shape has been refined using the EUHEDRAL macros [19] on the basis of the ambient temperature data, i.e. in the cubic paraphase. This crystal shape, transformed by the matrix [1/2 0 1/2][0 1 0][−1/2 0 1/2] to the orthorhombic setting, has been used to calculate a Gaussian absorption correction. The volume fractions of up to 12 different domains have been refined, based on the expected relative orientations of the domains [20]. These volume fractions were held fixed during the final refinement. Post-integration data processing and structure refinement have been carried out using Jana2000 [21]. Additional diffraction scans at zero detector position had ten fold increased exposure time. These scans are used to reconstruct the diffuse scattering intensity as a function of temperature. The reconstruction has been performed using software developed in-house (program RASTM).

3. Results and discussion

3.1. Bragg scattering

The topology of the CNO crystal structure can be described as the combination of two non-intersecting networks. The first such network is similar to the β-cristobalite structure with Cd replacing O and O(1) replacing Si. It can be interpreted as the superposition of Cd–O(1)–Cd zigzag chains parallel to the cubic ⟨110⟩ directions (figure 1). The second network consists of corner sharing NbO_6-octahedra. This network can be seen as the superposition of chains of octahedra running parallel to ⟨110⟩ (figure 1).

Structure refinement of CNO in SG $Ima2$ (tables 1 and 2) below its ferroelectric transition generally confirms

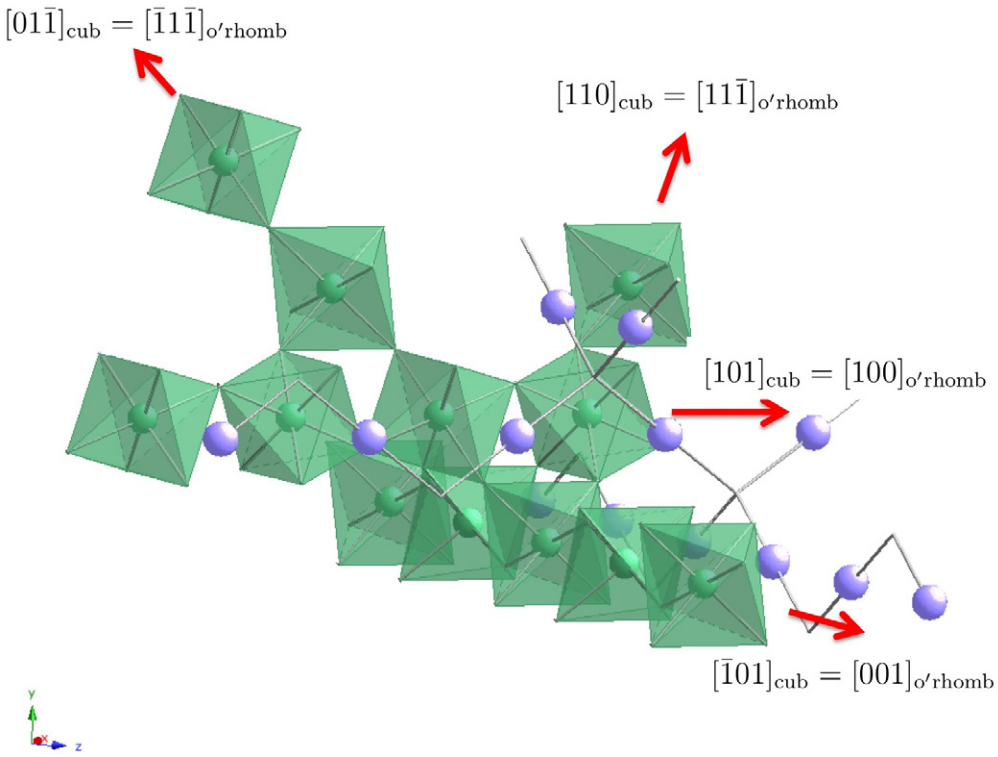

Figure 1. A fragment of the CNO structure. NbO_6-octahedra are shown in green, Cd-atoms in blue colour. O-atoms are not shown. Arrows indicate selected chain directions with indices referring to the cubic and to the orthorhombic cell setting (colour online).

the previous structure prediction conducted by *ab initio* methods [12]. Focusing on the individual $[NbO_5]$-chain directions, an ordering scheme of alternating long and short Nb–O bonds parallel [001] and ⟨111⟩ of the orthorhombic cell can be identified. Symmetric Nb–O bond distances prevail parallel to [100], i.e. along the octahedral chain direction normal to [001] (figure 1). These latter chains exclusively host the Nb(1) cation (figure 2). For the [001] chain direction at $T = 120$ K the O(2)–Nb(2)–O(2)′ bond distances are 1.888 and 2.042 Å; for the [100] chain direction the symmetric Nb(1)–O(3) bonds have a length of 1.96 Å. Along the $[1\bar{1}1]$ chain direction the succession of O(5)–Nb(2)–O(4)–Nb(1)–O(5) bond lengths is 1.917, 2.031, 1.921 and 2.006 Å at $T = 120$ K. These bond distances are in good agreement with those found by the *ab initio* calculations [12]. Figure 4 shows the temperature dependence of selected Nb–O bond distances. The pairwise short and long Cd(2)–O(1) distances remain almost constant at 2.22 and 2.26 Å in the orthorhombic phase. Cd(1)–O(1) remains symmetric at 2.245 Å, a value that is nearly identical to the bond distance at ambient temperature. The angle O(1)–Cd(2)–O(1)′ is 179.2° at 192 K and 176.2° at 98 K. The corresponding bridging angle at the Cd(1)-atom is 178° at 98 K.

Attempts to refine the structure at $T = 192$ K in the centrosymmetric SG *Imma* not only gave higher figures of merit ($R_{obs} = 0.057$), but also resulted in unrealistically large and anisotropic thermal displacement parameters (TDP) for some of the atoms.

Symmetry mode analysis (mode decomposition) has been performed in order to analyse the differences between the computed and the refined crystal structures as well as the general temperature trends. Towards this aim, the structure data (table 2) have been processed by the Web-based applications `AMPLIMODES` [22] and `ISODISPLACE` [23]. These programs analyse the distorted structure in terms of symmetry modes of the parent structure and then decompose the structural distortion, i.e. the individual displacement vectors, as a sum of the contributions from these symmetry modes. The cubic structure refined at $T = 220$ K is used to represent the cubic parent structure here. Differences in the results obtained with the two programs are due to differences in the way the origin is chosen. `AMPLIMODES` uses a convention that does keep the arithmetic centre of parent structure and distorted structure constant. `ISODISPLACE` chooses the origin such that the atomic displacements are minimized. The results of both calculation schemes are compared in figure 3.

The largest displacements are obtained for Nb, followed by Cd and the anions (table 3). Contrary to the *ab initio* calculations, the largest amplitude is found for the T_{2u}-mode, while the T_{1u}-mode is of minor importance down to $T = 98$ K (figure 3). Comparison of the results obtained from `AMPLIMODES` and `ISODISPLACE` show almost indistinguishable amplitudes for all modes, except for T_{1u}. As it is a polar mode, the amplitude of T_{1u} is expected to depend on the choice of origin. Linear extrapolation of the fourth power of the T_{2u} mode amplitude to zero yields $T_c = 194 \pm 2$ K (figure 3, inset). The corresponding power law behaviour of the mode amplitude is shown by the curve in figure 3. An effective (mean field) critical exponent of $1/4$ is common for continuous phase transitions with order–disorder contributions, often encountered in tricritical transitions.

Table 2. Refined structural parameters of CNO. Thermal displacement parameters are given in Å^2.

Atom	x	y	z	U_{11}	U_{22}	U_{33}	U_{12}	U_{13}	U_{23}	U_{eqv}
					$T = 292$ K, SG $Fd\bar{3}m$					
Nb	0	0	0	0.0130(1)	U_{11}	U_{11}	−0.000 30(1)	U_{12}	U_{12}	0.012 73(6)
Cd	1/2	x	x	0.0154(1)	U_{11}	U_{11}	−0.002 50(2)	U_{12}	U_{12}	0.015 44(5)
O1	5/8	x	x	0.0114(1)	U_{11}	U_{11}	0	0	0	0.0114(1)
O2	0.068 30(4)	7/8	y	0.0137(2)	0.0131(1)	U_{22}	0	0	−0.0046(1)	0.0133(1)
					$T = 220$ K, SG $Fd\bar{3}m$					
Nb	0	0	0	0.0131(1)	U_{11}	U_{11}	−0.000 17(1)	U_{12}	U_{12}	0.0131(1)
Cd	1/2	x	x	0.0141(1)	U_{11}	U_{11}	−0.002 09(2)	U_{12}	U_{12}	0.0141(1)
O1	5/8	x	x	0.0110(2)	U_{11}	U_{11}	0	0	0	0.0110(1)
O2	0.068 36(5)	7/8	y	0.0129(2)	0.0124(1)	U_{22}	0	0	−0.0037(1)	0.0126(1)
					$T = 192$ K, SG $Ima2$					
Cd1	0	0	0.507 77	0.0121(2)	0.0126(1)	0.0152(1)	−0.002 45(8)	0	0	0.0133(1)
Cd2	1/4	0.247 58(2)	0.253 63(5)	0.0160(2)	0.0135(1)	0.0126(2)	0	0	0.0032(1)	0.0140(1)
Nb1	0	0	0.000 67(7)	0.0132(3)	0.0131(3)	0.0144(2)	0.0006(1)	0	0	0.0136(2)
Nb2	1/4	0.755 62(3)	0.260 01(8)	0.0133(2)	0.0119(1)	0.0100(2)	0	0	−0.0017(1)	0.0117(1)
O1	1/4	0.3751(2)	0.0026(5)	0.012(1)	0.013(1)	0.008(1)	0	0	−0.001(1)	0.0111(6)
O2	1/4	0.8182(3)	0.5055(4)	0.013(1)	0.011(1)	0.011(1)	0	0	0.000(1)	0.0118(5)
O3	1/4	0.0681(3)	0.0041(4)	0.008(1)	0.012(1)	0.016(1)	0	0	0.000(1)	0.0117(6)
O4	0.9432(3)	0.1258(1)	0.8088(4)	0.013(1)	0.013(1)	0.013(1)	0.003(1)	0.000(1)	0.002(1)	0.0131(4)
O5	0.9441(3)	0.3752(2)	0.6961(4)	0.013(1)	0.013(1)	0.014(1)	−0.003(1)	0.000(1)	0.003(1)	0.0134(4)
					$T = 160$ K, SG $Ima2$					
Cd1	0	0	0.507 77	0.0118(2)	0.0133(3)	0.0141(2)	−0.0017(1)	0	0	0.0131(1)
Cd2	1/4	0.255 02(3)	0.264 44(8)	0.0152(2)	0.0128(1)	0.0114(2)	0	0	0.0027(1)	0.0131(1)
Nb1	0	0	0.0212(1)	0.0123(3)	0.0109(3)	0.0136(3)	0.000 77(8)	0	0	0.0123(2)
Nb2	1/4	0.739 15(5)	0.2553(1)	0.0113(2)	0.0102(1)	0.0093(2)	0	0	−0.0012(2)	0.0103(1)
O1	1/4	0.3749(2)	0.0122(7)	0.014(1)	0.010(1)	0.011(1)	0	0	0.003(1)	0.0118(7)
O2	1/4	0.8183(3)	0.5090(6)	0.015(2)	0.009(1)	0.016(2)	0	0	0.000(1)	0.0136(8)
O3	1/4	0.0681(3)	0.0105(6)	0.010(1)	0.011(1)	0.018(2)	0	0	−0.001(1)	0.0127(7)
O4	0.9455(4)	0.1240(2)	0.8193(5)	0.013(1)	0.010(1)	0.015(1)	0.002(1)	0.000(1)	0.002(1)	0.0125(5)
O5	0.9424(5)	0.3739(2)	0.7066(5)	0.014(1)	0.010(1)	0.015(1)	−0.004(1)	0.000(1)	0.002(1)	0.0131(4)
					$T = 120$ K, SG $Ima2$					
Cd1	0	0	0.507 77	0.0105(3)	0.0126(3)	0.0120(2)	−0.0012(1)	0	0	0.0117(1)
Cd2	1/4	0.243 50(4)	0.2502(1)	0.0132(2)	0.0117(2)	0.0101(2)	0	0	0.0027(1)	0.0117(1)
Nb1	0	0	− 0.0082(1)	0.0104(3)	0.0099(3)	0.0124(4)	0.0010(1)	0	0	0.0109(2)
Nb2	1/4	0.763 22(7)	0.2606(2)	0.0093(2)	0.0089(1)	0.0086(2)	0	0	−0.0010(2)	0.0089(1)
O1	1/4	0.3746(3)	0.0035(9)	0.013(2)	0.011(2)	0.011(2)	0	0	−0.002(1)	0.0114(9)
O2	1/4	0.8180(4)	0.5065(7)	0.012(2)	0.008(1)	0.017(2)	0	0	0.001(1)	0.0124(8)
O3	1/4	0.0669(4)	0.0064(6)	0.009(1)	0.009(1)	0.014(2)	0	0	−0.001(1)	0.0107(7)
O4	0.9425(5)	0.1262(2)	0.8083(6)	0.012(1)	0.010(1)	0.016(1)	0.003(1)	0.000(1)	0.003(1)	0.0126(5)
O5	0.9466(5)	0.3767(2)	0.6962(6)	0.012(1)	0.009(1)	0.016(1)	−0.002(1)	0.000(1)	0.003(1)	0.0126(6)
					$T = 98$ K, SG $Ima2$					
Cd1	0	0	0.507 77	0.0112(3)	0.0127(3)	0.0113(2)	−0.0011(1)	0	0	0.0117(2)
Cd2	1/4	0.256 99(5)	0.2665(1)	0.0132(2)	0.0119(2)	0.0098(2)	0	0	0.0018(1)	0.0116(1)
Nb1	0	0	0.0248(1)	0.0107(4)	0.0103(3)	0.0114(4)	0.0007(1)	0	0	0.0108(2)
Nb2	1/4	0.735 78(8)	0.2543(2)	0.0099(3)	0.0091(1)	0.0079(2)	0	0	−0.0009(2)	0.0090(1)
O1	1/4	0.3750(4)	0.013(1)	0.013(2)	0.015(2)	0.008(1)	0	0	0.001(1)	0.012(1)
O2	1/4	0.8177(4)	0.5073(7)	0.013(2)	0.008(1)	0.016(2)	0	0	0.001(1)	0.0122(9)
O3	1/4	0.0672(4)	0.0082(7)	0.012(1)	0.008(1)	0.013(1)	0	0	0.001(1)	0.0108(7)
O4	0.9461(6)	0.1234(2)	0.8185(6)	0.016(1)	0.009(1)	0.014(1)	0.002(1)	0.000(1)	0.002(1)	0.0129(6)
O5	0.9430(6)	0.3737(2)	0.7069(6)	0.014(1)	0.010(1)	0.015(1)	−0.003(1)	0.001(1)	0.002(1)	0.0130(6)

The symmetry mode analysis provides a remarkable improvement in detecting the static atomic displacements associated with the phase transition. Due to origin shifts encountered in the structure refinements, these displacements are not obvious by direct comparison of the structural coordinates shown in table 2. Referring all positions to a common origin, imposed by the parent phase, helps to obtain the actual displacements more clearly.

Figure 5 shows three displacement modes of the Nb-atom with exaggerated amplitudes [23]. These can be compared with the actual displacements observed at 120 K shown in figure 2(b). The T_{2u}-mode has positive and equal z and

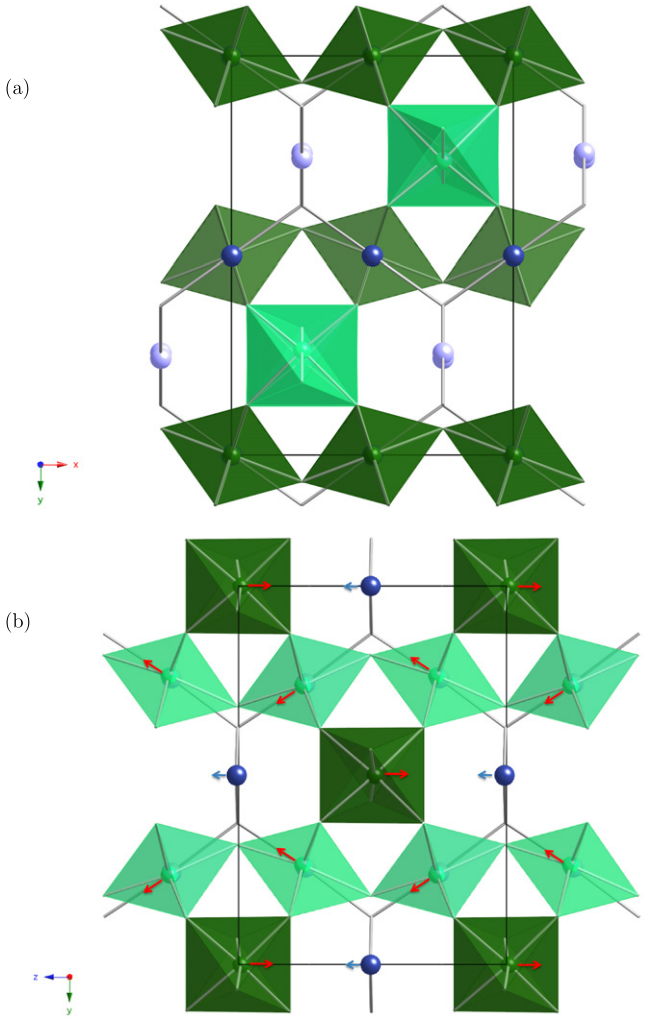

Figure 2. Refined CNO structure at $T = 120$ K (a) projected down [001] and (b) projected down [100]. Arrows indicate the displacement direction relative to the parent structure in (b). NbO_6-octahedra are shown in green, Cd-atoms in blue colour. Darker colours represent Nb(1) and Cd(1), lighter colours represent Nb(2) and Cd(2) (colour online).

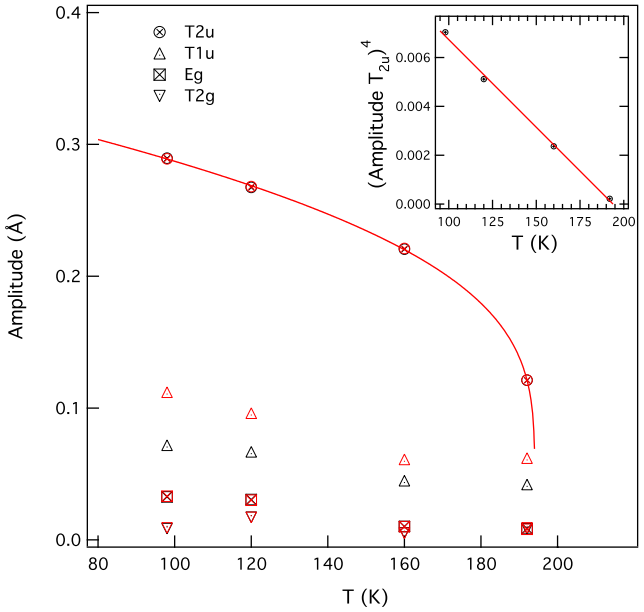

Figure 3. Total mode amplitudes as obtained with AMPLIMODES (black symbols) and with ISODISPLACE (larger values of T_{1u}, red symbols in the online version) as a function of temperature. The inset shows the linear extrapolation of the fourth power of the T_{2u} displacement mode amplitude.

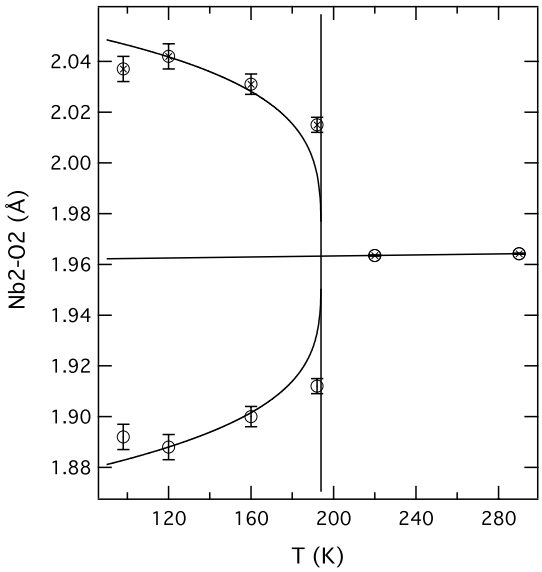

Figure 4. Refined Nb(2)–O(2) bond distances as a function of temperature. The perpendicular line marks the FE-phase transition temperature T_2, the straight line fit shows the extrapolated bond distance from the paraphase and the curves are guides to the eye.

y-components at the Nb(2)-site, while it contributes only a negative z-component at the Nb(1)-site (figure 5(a)). The first T_{1u}-mode causes displacements similar to the T_{2u}-mode at the Nb(2)-site (figure 5(b)). But it contributes a large z-component at the Nb(1)-site, of opposite sign with respect to the T_{2u}-mode. Thus a positive coupling of T_{1u} and T_{2u}-modes can effectively cancel the Nb(1)-displacement along [001], while retaining the polarization through the displacement of Nb(2). The second T_{1u}-mode leaves Nb(1) unaffected and displaces Nb(2) with a y-component opposite to that of the first T_{1u}-mode (figure 5(c)).

The results of the symmetry analysis indicate that the SM freezing at T_2 has T_{2u} symmetry. The associated mode in the paraphase is non-polar and therefore not nominally infrared (IR)-active. Because mode softening (of a T_{1u}-mode) has been observed above T_2 by IR-spectroscopy [8], this T_{1u}-mode might couple to the primary T_{2u}-mode. This would explain why the observed polar mode softening is incomplete.

The corresponding results obtained by the *ab initio* calculations [12], with the optimized cubic crystal structure as parent phase, indicate a total mode amplitude of 0.25 Å for the T_{1u}-mode and only about 0.03 Å for T_{2u}, which is approximately the reverse of the displacement amplitudes found in the structure refinements. The calculated phonon dispersion relation given in [12] included an unstable T_{2u}-mode, albeit with slightly higher imaginary frequency than the T_{1u}-mode used to generate the structural distortion. However,

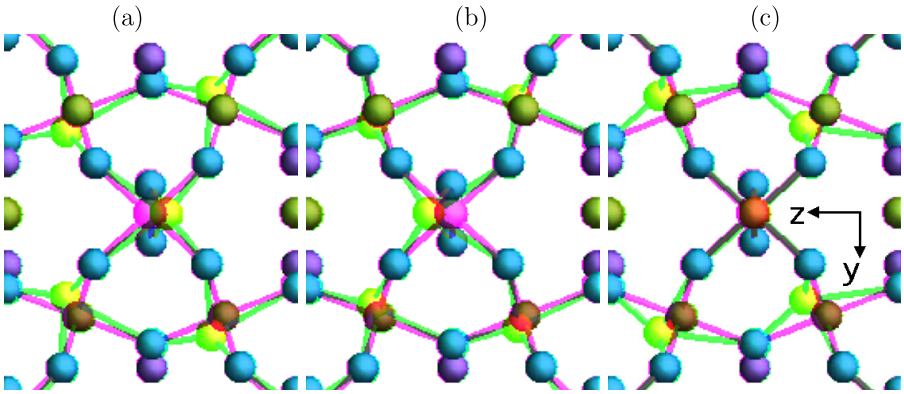

Figure 5. Selected Nb-displacement modes for the transition $Fd\bar{3}m \leftrightarrow Ima2$, projected along $[100]_{Ima2}$: (a) T_{2u} (b) $T_{1u}(E_u)$ (c) $T_{1u}(A_{2u})$. Displacement amplitudes are exaggerated. Yellow spheres with green bonds (lighter colours) indicate displaced Nb, magenta bonds (darker colours) indicate the parent structure (dark green = Cd, blue = O, dark red = Nb, colour online).

Table 3. Displacement modes at $T = 120$ K calculated using ISODISPLACE. IR_{site}: irreducible representation of the relevant site symmetry in the parent phase.

Mode	Atom	IR_{site}	Amplitude (Å)
A_{1g}	O(2)	A_1	−0.010(8)
E_g	O(2)	A_1	0.030(8)
T_{2g}	O(2)	A_1	−0.011(8)
T_{2g}	O(2)	B_2	0.01(1)
T_{2g}	O(2)	B_1	0.00(1)
T_{2g}	O(1)	T_2	0.00(1)
T_{1u}	Nb	A_{2u}	−0.032(15)
T_{1u}	Nb	E_u	0.023(15)
T_{1u}	Cd	A_{2u}	0.045(1)
T_{1u}	Cd	E_u	0.017(1)
T_{1u}	O(2)	A_1	0.045(8)
T_{1u}	O(2)	B_2	0.010(8)
T_{1u}	O(2)	B_1	0.052(8)
T_{1u}	O(1)	T_2	0.024(7)
T_{2u}	Nb	E_u	0.235(2)
T_{2u}	Cd	E_u	−0.108(9)
T_{2u}	O(2)	B_2	−0.067(8)
T_{2u}	O(2)	B_1	0.024(8)

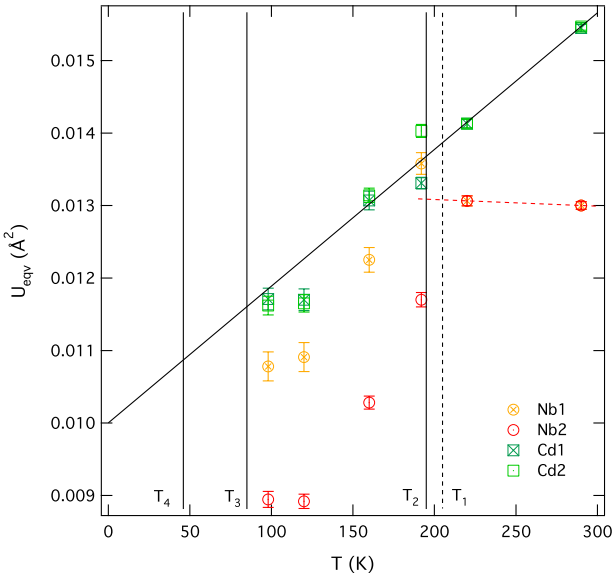

Figure 6. Equivalent isotropic thermal displacement of Nb- and Cd-atoms as a function of temperature. Phase transition temperatures are marked by vertical lines.

the *ab initio* calculations do not take finite temperature effects into account. Therefore a distortion of T_{1u} symmetry may well dominate at temperatures below T_3. In fact the critical softening temperature of the polar SM had been extrapolated to 60 K in [8].

Various authors have pointed out the role that disorder might play for the ferroelectric properties of CNO. Possible contributions of disorder can be judged by the size and temperature dependence of the thermal displacement parameters (TDPs) given in table 2. While Cd exhibits very large TDPs (figure 6), their temperature dependence does not deviate significantly from linear extrapolation of the temperature dependence in the cubic parent phase. Large and anisotropic thermal displacement of Cd is not unreasonable, given its linear coordination by two nearest neighbour O(1)-atoms. The observed temperature dependence of the thermal displacement parameters does not indicate a significant influence of the phase transitions at T_1 or T_2 on thermal displacement or local disorder of Cd, i.e. an annular motion of the Cd-atom as suggested in [16]. Contrary to this the relatively large TDP of the Nb-atom remains almost constant in the paraphase and into the FE-phase, indicating that the refined values within the paraelectric phase are dominated by disorder rather than harmonic thermal displacement. In the FE-phase, U_{eqv} at the Nb(2)-site rapidly decreases with temperature, as the T_{2u} distortion progresses. A similar temperature decay of U_{eqv} is delayed for the Nb(1)-site, which remains at higher levels of average displacement even at 98 K. Just below the FE transition the TDP at the Nb(1) site is comparable to the cubic phase. This indicates that some Nb disorder might remain at the Nb(1)-site far into the FE-phase. The obtained TDPs are systematically larger than reported ambient temperature data [14] by approximately 0.0045 Å^2, but the temperature gradients at the Cd and the Nb sites are comparable in both studies.

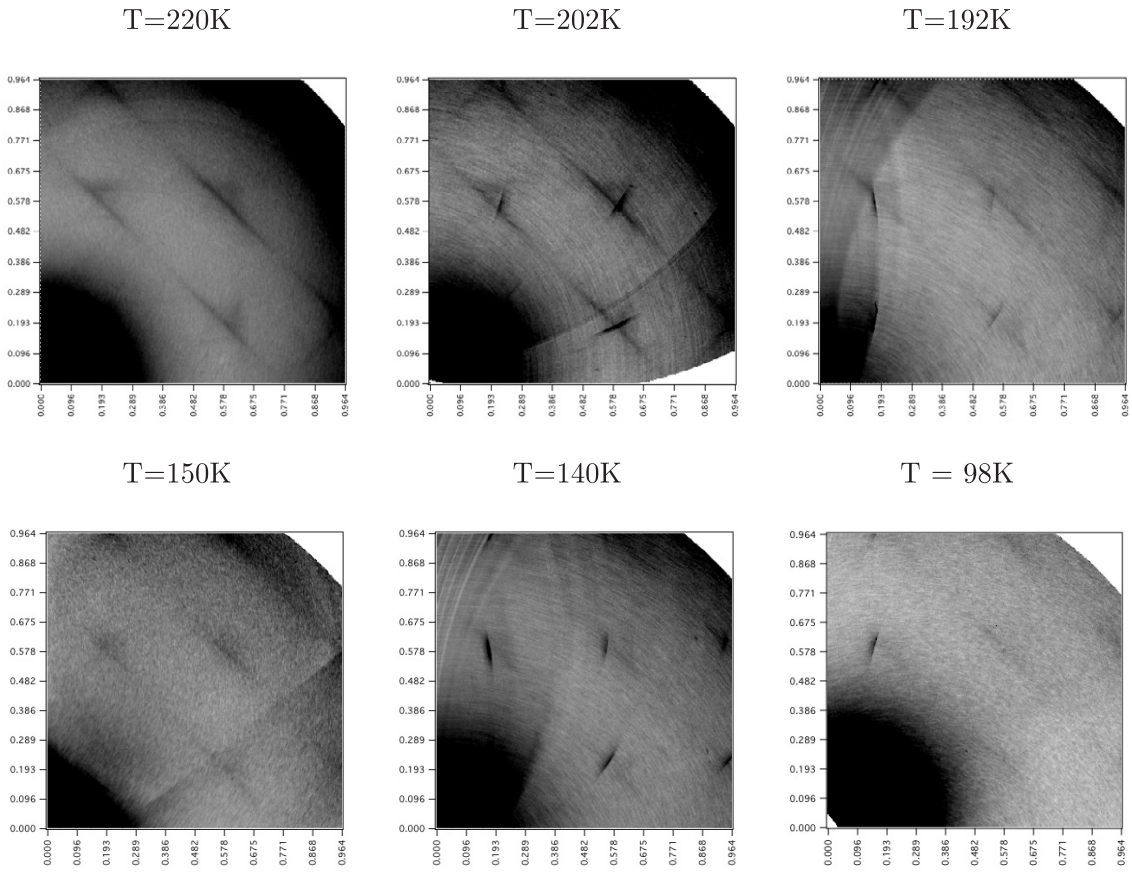

Figure 7. Diffuse scattering in sections $-3/2\ k\ l$ as a function of temperature. Axis dimensions are in Å^{-1}.

3.2. Diffuse scattering

Figure 7 shows a quadrant of a layer of reciprocal space at $h = -3/2$ with k and l ranging from 0 to 10. Intersections of diffuse scattering sheets normal to the cubic ⟨110⟩ directions with this layer show as linear streaks. Those sheets that intersect normal to the reciprocal layer result in relatively strong streaks, while those sheets intersecting at angles of 45° are broader and only faintly visible. Where individual layers intersect the diffuse scattering is enhanced, but apart from this no intensity modulation within the layers is discernible from our data. The simulation and interpretation of the diffuse scattering will be the subject of a different paper. Here it shall only be discussed in a qualitative manner and in relation to the observed temperature behaviour of the thermal displacement parameters. The intensity of the diffuse scattering is clearly above background level at 220 K and at 202 K, while it gradually decreases at lower temperatures. The trend of decreasing diffuse scattering intensity agrees with the parallel decrease in thermal displacement amplitude observed especially at the Nb(2)-site. In principle the diffuse scattering could serve as an indicator of the actual point group symmetry of the crystal. As the symmetry is lowered from cubic to orthorhombic symmetry, a reduction of the number of orientations of the diffuse layers would be expected, as it is observed in $KNbO_3$ [24], for example. The low temperature intensity decrease could therefore be interpreted as the result of symmetry reduction from cubic to orthorhombic. Due to the polydomain nature of the $Ima2$-phase, the orientations of the remaining diffuse layers average, resulting in a seemingly constant distribution of diffuse scattering across all possible orientations. The number of domains is expected to further increase below T_3 as a result of the transition to the postulated monoclinic phase.

In accordance with the computational results [12] it is the displacement of Nb that is of crucial importance for the FE-phase transitions in CNO. This displacement is driven by the d^0-character of Nb, mixing with the O 2p-states. In analogy to $KNbO_3$ [25] and $BaTiO_3$ [26, 27], Nb is likely to be disordered over several local energy minima within its octahedral coordination environment. At the same time the relative location of the local minima will be subject to distortions imposed by the displacive modes.

4. Conclusions

The crystal structure of CNO has been successfully refined in SG $Ima2$ based on a polydomain crystal and x-ray diffraction data. The primary order parameter for the T_2-transition is of T_{2u} symmetry and the distortion is dominated by Nb-displacement relative to the coordinating O(2)-anions. Polarization along [001] is possibly generated by coupling to a secondary distortion of T_{1u} symmetry. The phase transition at

$T_2 = 195$ K is of the improper ferroelectric type, as has been previously proposed for the transition at T_1 [5]. Nb disorder is expected to be significantly reduced by the transition to orthorhombic symmetry, as the number of available local minima is bound to decrease. The phase transition appears to have little influence on the thermal displacement and possible disorder of the Cd-atoms. The exact nature and symmetry of the intermediate state between T_1 and T_2 remains unresolved.

Acknowledgments

The CNO crystals have been prepared by I Glass in the group of R Miletich-Pawliczek (Universität Heidelberg). M Wilpsbäumer contributed to the diffraction experiments at beamline F1. S Heidrich kindly provided the microprobe analysis. The authors appreciate helpful comments by P Toledano (Amiens), regarding an earlier version of the manuscript, and by M Aroyo and D Orobengoa (Bilbao), on the use of AMPLIMODES in particular. Financial support by the Deutsche Forschungsgemeinschaft is gratefully acknowledged.

References

[1] Samara G A 2003 The relaxational properties of compositionally disordered ABO_3 perovskites *J. Phys.: Condens. Matter* **15** R367–411
[2] Cook W R and Jaffe H 1952 Ferroelectricity in oxides of fluorite structure *Phys. Rev.* **88** 1426
[3] Shirane G and Pepinsky R 1953 Dielectric properties and phase transitions of $Cd_2Nb_2O_7$ and $Pb_2Nb_2O_7$ *Phys. Rev.* **92** 504
[4] Tachibana M, Kawaji H and Atake T 2004 Calorimetric investigation of successive phase transitions in $Cd_2Nb_2O_7$ *Phys. Rev.* B **70** 064103
[5] Salaev F M, Kamzina L S and Kraĭnik N N 1992 Improper ferroelectric phase transition in cadmium pyroniobate *Sov. Phys.—Solid State* **34** 982–5
[6] Isupov V A 2005 On the nature of the phase transitions in cadmium pyroniobate *Phys. Solid State* **47** 2119–29
[7] Küster A 1992 Phasenübergänge bei ferroelektrischem $Cd_2Nb_2O_7$ und verwandten Substanzen *Dissertationsschrift*
[8] Buixaderas E, Kamba S, Petzelt J, Savinov M and Kolpakova N N 2001 Phase transitions sequence in pyrochlore $Cd_2Nb_2O_7$ studied by IR reflectivity *Eur. Phys. J.* B **19** 9–16
[9] Samara G A, Venturini E L and Boatner L A 2006 Dielectric properties and phase transitions of $Cd_2Nb_2O_7$: effects of pressure and temperature *J. Appl. Phys.* **100** 074112
[10] Taniguchi H, Shimizu T, Kawaji H, Atake T, Itoh M and Tachibana M 2008 Ferroelectric phase transition of $Cd_2Nb_2O_7$ studied by Raman scattering *Phys. Rev.* B **77** 224104
[11] Hulme J K 1953 Low-temperature dielectric properties of cadmium and lead niobates *Phys. Rev.* **92** 504
[12] Fischer M, Malcherek T, Bismayer U, Blaha P and Schwarz K 2008 Structure and stability of $Cd_2Nb_2O_7$ and $Cd_2Ta_2O_7$ explored by *ab initio* calculations *Phys. Rev.* B **78** 014108
[13] Weller M T, Hughes R W, Rooke J, Knee C S and Reading J 2004 The pyrochlore family—a potential panacea for the frustrated perovskite chemist *Dalton Trans.* **2004** 3032–41
[14] Lukaszewicz K, Pietraszko A, Stepiendamm J and Kolpakova N N 1994 Temperature-dependence of the crystal-structure and dynamic disorder of cadmium in cadmium pyroniobates $Cd_2Nb_2O_7$ and $Cd_2Ta_2O_7$ *Mater. Res. Bull.* **29** 987–92
[15] Malcherek T 2007 Anisotropic diffuse x-ray scattering in early transition metal oxide structures *J. Phys.: Condens. Matter* **19** 275208
[16] Paściak M, Wołcyrz M, Pietraszko A and Leoni S 2010 Local structure in the paraelectric phase of $Cd_2Nb_2O_7$ determined from x-ray diffuse scattering, by means of *ab initio* molecular dynamics and Monte Carlo modeling *Phys. Rev.* B **81** 014107
[17] Meldrum A, White C W, Keppens V, Boatner L A and Ewing R C 2001 Irradiation-induced amorphization of $Cd_2Nb_2O_7$ pyrochlore *Phys. Rev.* B **63** 104109
[18] Kabsch W 1993 Automatic processing of rotation diffraction data from crystals of initially unknown symmetry and cell constants *J. Appl. Crystallogr.* **26** 795–800
[19] Lutz M and Schreurs A M M 2008 http://www.crystal.chem.uu.nl/distr/euhedral
[20] Flack H D 1987 The derivation of twin laws for (pseudo-)merohedry by coset decomposition *Acta Crystallogr.* A **43** 564–8
[21] Petricek V, Dusek M and Palatinus L 2000 *Jana2000. The Crystallographic Computing System* (Praha, Czech Republic: Institute of Physics)
[22] Orobengoa D, Capillas C, Aroyo M I and Perez-Mato J M 2009 *AMPLIMODES*: symmetry-mode analysis on the Bilbao crystallographic server *J. Appl. Crystallogr.* **42** 820–33
[23] Campbell B J, Stokes H T, Tanner D E and Hatch D M 2006 ISODISPLACE: a web-based tool for exploring structural distortions *J. Appl. Crystallogr.* **39** 607–14
[24] Comès R and Shirane G 1972 Neutron-scattering analysis of the linear-displacement correlations in $KTaO_3$ *Phys. Rev.* B **5** 1886–91
[25] Comès R, Lambert M and Guinier A 1970 Désordre linéaire dans les cristaux (cas du silicium, du quartz, et des pérovskites ferroélectriques) *Acta Crystallogr.* A **26** 244–54
[26] Chaves A S, Barreto F C S, Nogueira R A and Zẽks B 1976 Thermodynamics of an eight-site order–disorder model for ferroelectrics *Phys. Rev.* B **13** 207–12
[27] Zalar B, Lebar A, Seliger J, Blinc R, Laguta V V and Itoh M 2005 NMR study of disorder in $BaTiO_3$ and $SrTiO_3$ *Phys. Rev.* B **71** 064107